medium varying transverse to the direction of propagation," *IEEE Trans. Quantum Electron.* (Corresp.), vol. QE-10, pp. 465–467, April 1974.
[19] D. Marcuse, *Light Transmission Optics*. New York: Van Nostrand, 1972.
[20] J. G. Dil and H. Blok, "Propagation of electromagnetic surface waves in a radially inhomogeneous optical waveguide," *Opt. Electron.*, vol. 5, pp. 415–428, 1973.
[21] K. S. Miller, "The one-sided Green's function," *J. Appl. Phys.*, vol. 22, pp. 1054–1057, August 1951.

Slow-Wave Propagation Along Variable Schottky-Contact Microstrip Line

DIETER JÄGER

Abstract—**Schottky-contact microstrip lines (SCML) are a special type of transmission line on the semiconducting substrate: the metallic-strip conductor is specially selected to form a rectifying metal–semiconductor transition while the ground plane exhibits an ohmic metallization. Thus the cross section of SCML is similar to that of a Schottky-barrier diode. The resulting voltage-dependent capacitance per unit length causes the nonlinear behavior of such lines.**

In this paper a detailed analysis of the slow-wave propagation on SCML is presented, including the effect of metallic losses. Formulas for the propagation constant and characteristic impedance are derived and an equivalent circuit is presented. Conditions for slow-mode behavior are given, particularly taking into account the influence of imperfect conductors and defining the range of many interesting applications. Experimental results performed on Si-SCML are compared with theory.

I. Introduction

DUE to particular applications in microwave integrated circuits, microstrip lines on semiconductor substrates have been thoroughly investigated both in theoretical and experimental works during the last few years. The Schottky-contact microstrip line (SCML) is a special form of microstrip line on a semiconducting substrate: the cross section [Fig. 1(a)] is similar to a Schottky-barrier diode; i.e., the stripline forms a rectifying metal–semiconductor transition to the chip with a large-area ohmic-contact back metallization. At the Schottky-barrier contact a depletion layer arises, the depth of which depends strongly on the applied voltage. Thus the most interesting features of SCML's are caused by this voltage-dependent depletion-layer capacitance per unit length. Two modes of operation may be distinguished: the large-signal behavior, which is characterized by nonlinear wave propagation, and the small-signal properties, which are determined by bias-dependent transmission-line parameters.

The wave propagation on SCML's has been investigated recently, leading to several fundamental results: large-signal operation leads to distributed harmonic frequency generation and the possibility of parametric amplification [1], [2]. Under small-signal conditions a slow-wave propagation occurs, and the propagation constant and characteristic impedance may be changed by an external dc bias [3], [4]. In particular, it has been verified that bias-dependent phase delay gives rise to possible applications of SCML in variable IC microwave components, such as resonators, delay lines, phase shifters, or tunable filters [5]–[7].

To a certain extent the SCML resembles the microstrip line, which serves as the electrical-interconnection pattern in IC technology on MOS or MIS systems where an oxide layer insulates the semiconductor wafer from the metallic conductors. The high-frequency behavior has been investigated by several workers, since the propagation delay imposes a limitation upon signal velocity [8]–[11]. Introducing the voltage-dependent capacitance of the MIS system, a variable (nonlinear) MIS microstrip line results [12], [13]. The fundamental theoretical work on wave propagation along such transmission lines has been done by Guckel *et al.* [8], assuming perfect conductors and a large ratio $r = w/l$ of strip width w to substrate thickness l.

Until now an accurate calculation of the influence of imperfect metallic conductors has been neglected in theoretical analysis. The experimental results, however, show large deviations from theory, especially in the lower slow-mode region [4], [11] which exhibits the most interesting features for possible applications. The efficiency of harmonic-frequency conversion and parametric amplification in nonlinear SCML depends strongly on the metallic losses [1], [2], and the phase delay of the variable SCML is influenced by the additional attenuation. In this way, the influence of the metallic losses has become a central problem in the discussion of possible practical applications.

In this paper, a more detailed analysis of small-signal slow-wave propagation along variable SCML is presented, including the effect of imperfect conductors. The treatment

Manuscript received December 2, 1975; revised February 25, 1976. This work was supported by the Deutsche Forschungsgemeinschaft under Grant Ha 505/6/10.
The author is with the Institute for Applied Physics, University of Münster, 4400 Münster, Germany.

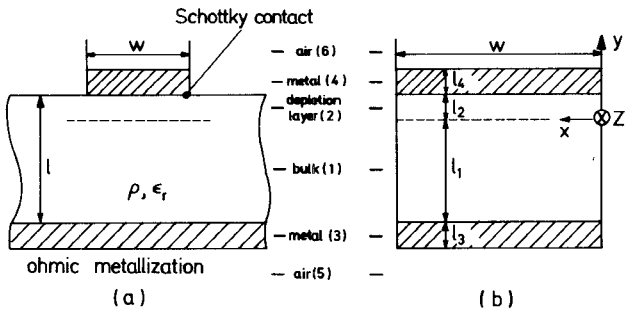

Fig. 1. Schottky-contact microstrip line. (a) Cross section. (b) Parallel-plate waveguide model.

is based upon the work of Guckel *et al.* [8] and confined to the slow-mode region. Formulas are derived in the limit of a parallel-plate waveguide approach and an equivalent circuit is introduced. The slow-mode region is restricted due to metallic losses, and the characteristic frequencies are given. Finally, the theoretical results are compared with experimental values. The influence of fringing fields in the case of real SCML are not considered, since it may be calculated as in [4].

II. Parallel-Plate Waveguide Model

Fig. 1(a) shows the cross section of the SCML. The ohmic back metallization forms the ground plane. The Schottky contact is realized by the strip conductor of width w in intimate contact with the semiconductor of thickness l, doping concentration n_D (here n-type), resistivity ρ, and relative permittivity ε_r. A depletion layer is generated a depth l_2, which depends on the applied reverse bias V according to the well-known equation [14]

$$l_2 = \sqrt{\frac{2\varepsilon_0\varepsilon_r(V + V_D)}{en_D}} \tag{1}$$

where e is the elementary charge, ε_0 the free-space permittivity, and V_D the barrier potential of the Schottky barrier. In the following, l_2 has to be considered bias-dependent and the RF amplitudes to be small enough to allow the use of (1).

Fig. 1(b) shows the parallel-plate waveguide model of the SCML assuming $w \gg l$, so the fringing fields may be neglected. The following six layers have to be considered. The first layer is the semiconducting bulk with thickness l_1 and resistivity ρ. The second layer is represented by the depletion layer, with thickness l_2 and a negligible conductivity at microwave frequencies, since the concentration of free charge carriers is considerably reduced. The two metallic layers are formed by the conductors with thicknesses l_3 and l_4 and conductivities σ_3 and σ_4. The fifth and sixth layers are given by the surrounding air. For such a multilayered transmission line, the fundamental mode of electromagnetic-wave propagation is a TM mode which is a surface wave. Propagation in the z direction is characterized by the complex propagation constant $\gamma = \alpha + j\beta$, according to $\exp(-\gamma z)$ and the time factor $\exp(j\omega t)$. By using the Maxwellian equations the field components of the ith layer are given by

$$H_{xi}(y) = a_{+i}\exp(\gamma_i y) + a_{-i}\exp(-\gamma_i y)$$

$$E_{yi}(y) = -\frac{\gamma}{j\omega\varepsilon_0\varepsilon_i}H_{xi}(y),$$

$$E_{zi}(y) = -\frac{\gamma_i}{j\omega\varepsilon_0\varepsilon_i}(a_{+i}\exp(\gamma_i y) - a_{-i}\exp(-\gamma_i y)),$$

$$i = 1,\cdots,6 \tag{2}$$

where the $a_{\pm i}$ are complex amplitudes, γ_i denotes the transverse propagation constants in the y direction, and $\varepsilon_i = \varepsilon_{ri} - j\sigma_i/(\omega\varepsilon_0)$, the complex permittivity of the ith layer. The separation conditions are formulated as follows:

$$\gamma_i^2 + \gamma^2 = -k_0^2\varepsilon_i, \qquad i = 1,\cdots,6 \tag{3}$$

where $k_0^2 = \omega/c$, with $c = 1/\sqrt{\mu_0\varepsilon_0}$ the free-space speed of light. At the boundaries $y = 0$, l_2, $l_2 + l_4$, $-l_1$, $-(l_1 + l_3)$ the electromagnetic continuity conditions must be satisfied, which, together with (3), gives

$$\frac{\gamma_1}{j\omega\varepsilon_0\varepsilon_1}\tanh\gamma_1 l_1 + \frac{\gamma_2}{j\omega\varepsilon_0\varepsilon_2}\tanh\gamma_2 l_2 + M(\gamma_1,\cdots,\gamma_6) = 0. \tag{4}$$

In this equation the quantity M signifies the "metal function"

$$M = \sum_{i=3}^{6} Z_i t_i + \sum_{\substack{(i,j,k)=1 \\ n_i<n_j<n_k}}^{6} \frac{Z_i Z_k}{Z_j} t_i t_j t_k + \sum_{\substack{(i,j,k,l,m)=1 \\ n_i<n_j<n_k<n_l<n_m}}^{6} \frac{Z_i Z_k Z_m}{Z_j Z_l} t_i t_j t_k t_l t_m \tag{5}$$

with $t_i = \tanh\gamma_i l_i$ for $i = 1,\cdots,4$, $t_5 = t_6 = 1$, and $n_i = i(-1)^i$. Z_i denotes the characteristic field impedance

$$Z_i = \frac{\gamma_i}{j\omega\varepsilon_0\varepsilon_i}, \qquad i = 1,\cdots,6. \tag{6}$$

The summation in (5) has to be done as follows [10]. In the second sum such triplets (i,j,k) are selected from the numbers $1,\cdots,6$, for which $n_i < n_j < n_k$ is fulfilled. The twenty terms are added up. The third sum is handled in a similar manner, yielding six terms.

The eigenvalue equation (4) is the same as in [8], except for the term M which vanishes in the case of perfect conductors. Thus, by use of the separation conditions, (4) may be rewritten as

$$\gamma^2 = \frac{-k_0^2\left[\frac{1}{\gamma_1}\tanh\gamma_1 l_1 + \frac{1}{\gamma_2}\tanh\gamma_2 l_2\right] + j\omega\varepsilon_0 M}{\frac{1}{\gamma_1\varepsilon_1}\tanh\gamma_1 l_1 + \frac{1}{\gamma_2\varepsilon_2}\tanh\gamma_2 l_2}. \tag{7}$$

In regard to the numerical solution of (4), the transverse propagation constants γ_i $(i = 2,\cdots,5)$ are expressed in terms of γ_1 with the help of (3). The zeros are then found by Newton's iteration procedure. The results are illustrated in Fig. 2(a) and (b) for attenuation constant α and normalized wavelength λ_0/λ, respectively, where λ_0 denotes the

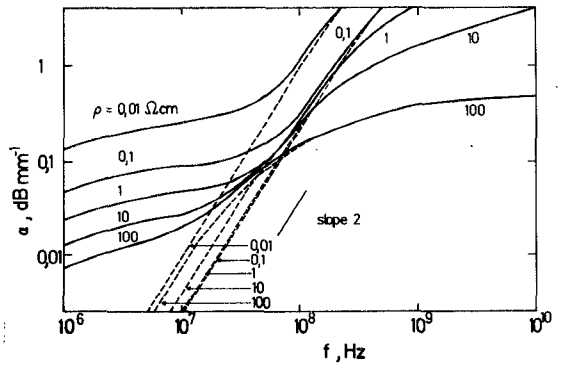

(a)

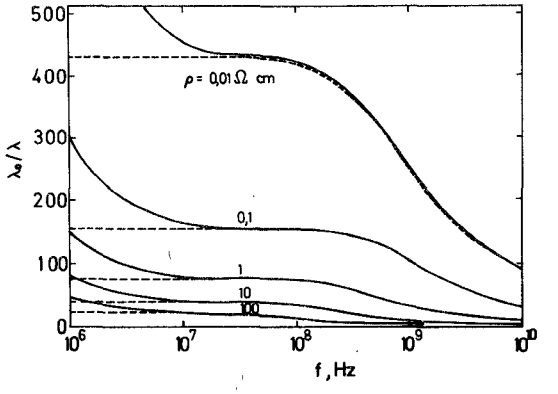

(b)

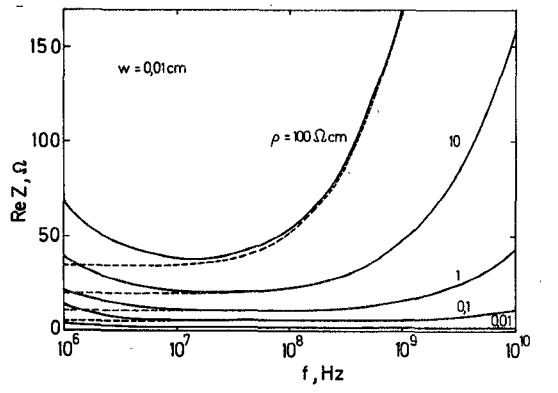

(c)

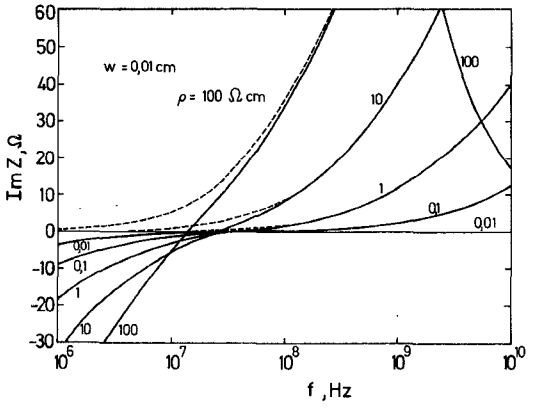

(d)

Fig. 2. Numerical results of transmission-line parameters. (a) Attenuation constant. (b) Slowing factor. (c) Real part. (d) Imaginary part of characteristic impedance. n–Si substrate, $l = 0.022$ cm, $l_3 = l_4 = 5$ μm, $V + V_D = 0.8$ V, $\varepsilon_r = 11.7$. Parameter is the resistivity of Si. ——: imperfect conductors with $\sigma_m = 3.5 \cdot 10^5$ Ω^{-1} cm^{-1}. – – – –: perfect conductors.

free-space wavelength. The semiconductor resistivity is a parameter. The dielectric constant and mobility are those of the Si substrate, needed to calculate the required values of the doping concentration in (1). A fixed value $V + V_D = 0.8$ V is chosen as the Schottky-contact potential corresponding to a typical barrier potential $V_D = 0.5$ V of n-type Si-Schottky barriers and a reverse bias $V = 0.3$ V. Thickness and conductivity of the metallic layers are common values for microminiaturized Al conductors. The dotted lines show the case where $M = 0$ for perfect conductors. Assuming lossless conductors, the slow-mode region is defined by a frequency-independent phase velocity v, which is very small as compared with c. In Fig. 2(b), $\lambda_0/\lambda > 400$ for the $\rho = 0.01$-$\Omega \cdot$ cm substrate. Within this frequency range the attenuation would be proportional to the square of the frequency; cf. Fig. 2(a). By this definition the slow-mode region is confined by an upper frequency limit only (for $M = 0$).

As can be seen from Fig. 2, the transmission-line parameters are strongly influenced by the metallic losses in the lower frequency range. The attenuation constant is considerably enhanced and the phase velocity exhibits dispersion. It may be concluded therefore that the slow-mode region as previously defined must be restricted by a lower frequency limit.

Equation (7) may be interpreted on the basis of transmission-line theory [5]. Then the numerator represents the series impedance W' and the denominator the shunt admittance Y' per unit length of a T-equivalent circuit. Thus the characteristic impedance Z of the SCML can be evaluated from

$$Z = (W'/Y')^{1/2} \tag{8}$$

in a way similar to that previously shown.

The numerical results of Re Z and Im Z are plotted in Fig. 2(c) and (d), respectively. Again the transmission-line parameters are strongly influenced by imperfect conductors within the lower frequency range: Re Z becomes frequency dependent and Im Z negative. In the case of lossless conductors, the slow-mode region is characterized by frequency independent Re Z.

III. Influence of Imperfect Conductors

In the following some approximate expressions for the transmission-line parameters under slow-mode conditions are derived. In particular, the term M in (7) has to be calculated. Since it is difficult to make approximations from (5) with the help of the previous treatment, an analogous procedure, based upon the transverse resonant method [15] which has already been employed in [8], [10], is used.

In the six-layer configuration of Fig. 1(b), the characteristic impedance $Z_0 = 377$ Ω of the air layers is first transformed through the metallic layers by common transmission-line theory. This yields the y-directed field impedances Z_t at the boundaries $y = -l_1$ and $y = l_2$. In the following, for simplicity, conductors identical with $l_3 = l_4 = l_m$ and $\sigma_3 = \sigma_4 = \sigma_m$ are assumed. If $l_m \gtrsim 0.1$

μm, Z_t is approximately

$$Z_t(y = -l_1,l_2) = Z_m \coth \gamma_m l_m \tag{9}$$

with

$$\gamma_m = \frac{1+j}{\delta_m}$$

and

$$Z_m = \frac{1+j}{\delta_m \sigma_m} \tag{10}$$

where $\delta_m = [2/(\mu_0 \sigma_m \omega)]^{1/2}$ is the skin depth of the metallic layers. Equation (9) is a reasonably good approximation for typical values of σ_m. In this case, the influence of the air layers has disappeared and a four-layered configuration results. Now Z_t is transformed through the depletion layer and the bulk material to the plane $y = 0$. Then the resonance condition finally yields

$$\sum_{i=1}^{2} Z_i \tanh \gamma_i l_i + Z_m \coth \gamma_m l_m (2 - \tanh^2 \gamma_1 l_1) = 0 \tag{11}$$

if

1) $|Z_2| \gg |Z_m \coth \gamma_m l_m \tanh \gamma_2 l_2|$;
2) $l_m \gtrsim 0.1$ μm;
3) $\omega < \omega_s = \dfrac{2}{\mu_0 \sigma l_1^2}$;
4) $\sigma l_1 \lesssim 0.1 \sigma_m \min (l_m, \delta_m)$. (12)

The first and second conditions are satisfied in the case of the typical SCML for microelectronic applications. The third and fourth conditions ensure that the longitudinal component of the current within the semiconductor is less than the current through the strip conductor. ω_s is the frequency at which l_1 equals the skin depth of the semiconductor.

Equation (11) yields the desired expression for M of (4)

$$M = W_m(2 - \tanh^2 \gamma_1 l_1) \tag{13}$$

with

$$W_m = Z_m \coth \gamma_m l_m = \begin{cases} \dfrac{1}{\sigma_m l_m} + j \dfrac{l_m \mu_0 \omega}{3}, & \text{for } \delta_m \gtrsim 2 l_m \\ \dfrac{1+j}{\sigma_m \delta_m}, & \text{for } 2\delta_m \lesssim l_m. \end{cases}$$

The slow-mode region may be defined for frequencies [4]

$$\omega \lesssim 0.3\omega_c = 0.3\sqrt{3}\,(\omega_p^{-1} + \tfrac{2}{3}\omega_s^{-1})^{-1} \tag{14}$$

with

$$\omega_p = \omega_d \frac{l_2}{l_1}$$

and

$$\omega_d = \frac{\sigma}{\varepsilon_r \varepsilon_0}. \tag{15}$$

ω_d designates the dielectric relaxation frequency and ω_p the characteristic frequency limit for interfacial polarization

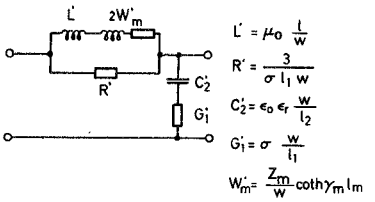

Fig. 3. Equivalent circuit and circuit parameters.

of the two-layered semiconductor substrate. Within the slow-mode region of (14) the hyperbolic functions in (7) may be expanded, assuming $l_1 \gg l_2$, [5], [8]

$$\gamma^2 = \frac{j\omega\mu_0 l(1 - W_m \sigma l_1) + \frac{1}{3}\omega^2 \mu_0^2 \sigma l_1^3 (1 - 2W_m \sigma l_1) + 2W_m}{l_1 \sigma^{-1} + (j\omega\varepsilon_0\varepsilon_r)^{-1} l_2}. \tag{16}$$

Finally, from the viewpoint of transmission-line theory, this equation yields the equivalent circuit in Fig. 3 and the following approximations, if $|W_m \sigma l_1| \ll 1$, is used:

$$\gamma = jk_0 \sqrt{\varepsilon_r \frac{l}{l_2}} \left[1 - j\left(\sqrt{3}\,\frac{\omega}{\omega_c} + \frac{2W_m}{\omega\mu_0 l}\right)\right]^{1/2} \tag{17}$$

$$Z = \frac{Z_0}{w} \sqrt{\frac{l l_2}{\varepsilon_r}} \left[1 + j\left(\frac{\omega}{\omega_p} - \frac{2}{3}\frac{\omega}{\omega_s} - \frac{2W_m}{\omega\mu_0 l}\right)\right]^{1/2}. \tag{18}$$

L' of Fig. 3 represents the common inductance per unit length of the parallel-plate waveguide and $2W_m'$ the influence of the two metallic conductors. The resistance R' per unit length accounts for longitudinal losses in the semiconductor due to the electric-field component in the direction of propagation. The effective height $l_1/3$ is caused by a current density not being constant in the transversal plane: from (2), (3), and (17) it can be verified that E_{z1} varies linearly with y [5], [11], a sufficiently good approximation under slow-mode conditions. C_2' is identical with the depletion-layer capacitance and G_1' with the semiconductor bulk conductance per unit length. A more general equivalent circuit is obtained if L' is replaced by $L'(1 - W_m \sigma l_1)$, (16), provided that the longitudinal current through the semiconductor is not neglected in comparison with that through the adjacent metallic ground plane. Moreover, the parallel circuit of L' and R' in Fig. 3 is in accordance with the physical mechanism of current transport along such layered lines. Thus it is evident that the attenuation due to series losses in the semiconductor is proportional to the square of frequency, a fact that gave rise to much confusion in the literature [8], [11].

The desired slow-wave properties of the SCML may now be deduced from (17) and (18), if W_m may be neglected

$$\alpha \sim \omega^2, \qquad v = c\left[\frac{2\varepsilon_0(V + V_D)}{\varepsilon_r l^2 e n_D}\right]^{1/4} \tag{19}$$

$$\operatorname{Re} Z = \frac{Z_0}{w}\sqrt{\frac{1}{\varepsilon_r}}\left[\frac{2\varepsilon_r\varepsilon_0(V + V_D)}{e n_D}\right]^{1/4}. \tag{20}$$

The attenuation becomes a minimum for

$$\sigma = \sigma_{\min} = \left(\frac{9\varepsilon_0\varepsilon_r}{2\mu_0^2 l_1^2 (V + V_D)\mu_n}\right)^{1/3}. \tag{21}$$

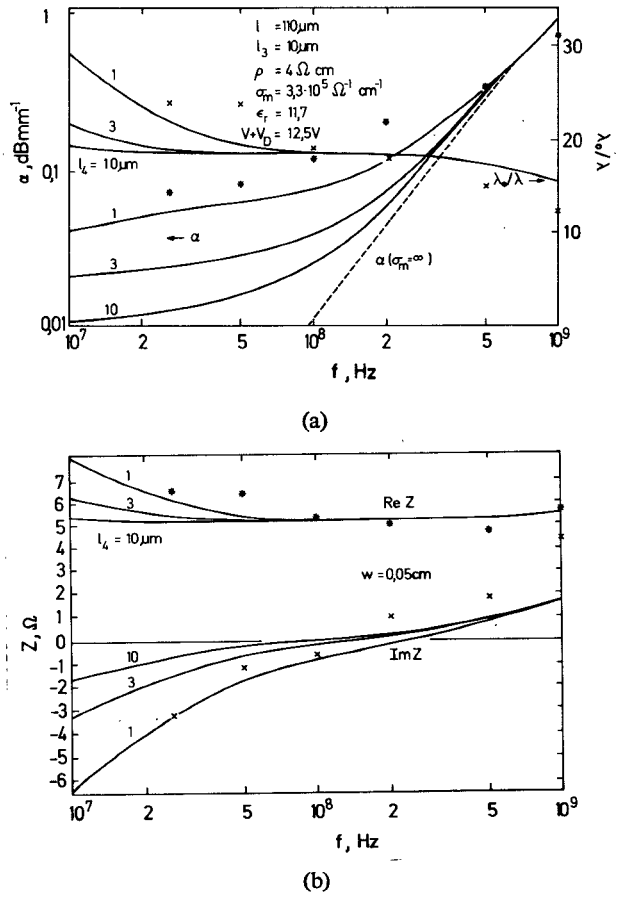

Fig. 4. Transmission-line parameters versus frequency; parameter is the strip-conductor thickness. (a) Attenuation constant and slowing factor. (b) Characteristic impedance, experimental points of SCML-4 [4].

Altogether, ω_c gets a maximum value and $\operatorname{Im} Z \approx 0$; cf. Fig. 2. These are the most attractive features of the SCML: the phase velocity v is very small compared with c, and v and $\operatorname{Re} Z$ are voltage dependent and exhibit no dispersion.

Fig. 4 shows detailed plots of transmission-line parameters influenced by the finite metallic conductivity calculated as in Section II. As can be seen, the slow-mode properties, as defined by (19) and (20), can only be obtained for frequencies $\omega_{m1} \lesssim \omega \lesssim 0.3\omega_c$. This lower frequency limit ω_{m1} may be evaluated from (17) and (18)

$$\omega_{m1} \approx \begin{cases} \left[\dfrac{9}{\sigma_m \mu_0 l l_m}\,\omega_c\right]^{1/2}, & \text{for } \delta_m \gtrsim 2l_m \\ \left[\dfrac{40}{\sigma_m \mu_0 l^2}\,\omega_c^2\right]^{1/3}, & \text{for } l_m \gtrsim 2\delta_m. \end{cases} \quad (22)$$

For the practical example $f_c = 1$ GHz, $l = 0.2$ mm, and $\sigma_m = 3.3 \cdot 10^5\ \Omega^{-1}\ \mathrm{cm}^{-1}$, one obtains $f_{m1} \approx 150$ MHz if $l_m \gtrsim 14\ \mu$m so that $l_m > 2\delta_m$. From (17) and (18) a second lower frequency limit may be derived so that for $\omega_{m2} \lesssim \omega \lesssim 0.3\omega_c$ only v and $\operatorname{Re} Z$ exhibit slow-mode properties

$$\omega_{m2} = \begin{cases} \omega_{m1}^2/\omega_c, & \text{for } \delta_m \gtrsim 2l_m \\ \omega_{m1}^3/\omega_c^2, & \text{for } l_m \gtrsim 2\delta_m. \end{cases} \quad (23)$$

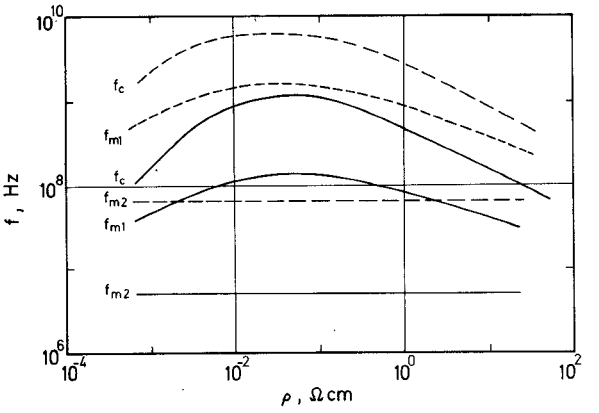

Fig. 5. Frequency limits for slow-mode region versus resistivity of n–Si: $V + V_D = 0.5$ V and $\sigma_m = 3.3 \cdot 10^5\ \Omega^{-1}\ \mathrm{cm}^{-1}$. Parameter is the substrate thickness: —— $l = 0.02$ cm; - - - - $l = 0.005$ cm.

For the above-mentioned example, $f_{m2} \approx 5$ MHz if now $l_m \gtrsim 80\ \mu$m.

In Fig. 5 the three frequency limits are given as a function of semiconductor resistivity, when $l_m \geq 2\delta_m$ is assumed. The significance of imperfect conductors is evident. A substrate thickness $l = 50\ \mu$m, for example, results in $f_{m1} \gtrsim 0.3 f_c$ so that the slow-mode region has nearly disappeared.

IV. Experimental Study

In the following, a quantitative comparison is carried out between experimental values and the presented theory; i.e., the equivalent circuit of Fig. 3. Fringing fields will not be considered. This may be done, however, in a quasi-static approximation by introducing spreading factors for the elements of the equivalent circuit [4], similar to W_m from [16].

SCML's with Al and Au Schottky contacts are prepared on n–Si wafers; a sample preparation is described in [4]. The measured reverse voltage-capacitance characteristic agrees well with (1). The values of barrier height as determined from the saturation current density under forward bias correspond with those given in [14], thus confirming the good properties of the rectifying metal–semiconductor transition with diffusion potentials V_D between 0.5 and 0.6 V.

Z and γ are determined by measurements of the open-circuit and short-circuit input impedance of the SCML. An immitance and transfer-function bridge is used. Experimental values of sample SCML-4 from [4], with $\rho = 4\ \Omega \cdot$ cm, $l = 0.11$ mm, $l_3 = 8\ \mu$m, $l_4 = 1.5\ \mu$m, $w = 0.055$ cm, and Al–n–Si Schottky contact, are given in Fig. 4. Bias is 12 V. A comparison with the theoretical curves show only small differences between experimental values and theory. These differences, however, may be traced back to a smaller actual conductivity of the vacuum-evaporated conductors than that of Al bulk material which has been used in the theoretical calculation. Thus the agreement with theory is satisfactory, bearing in mind the large

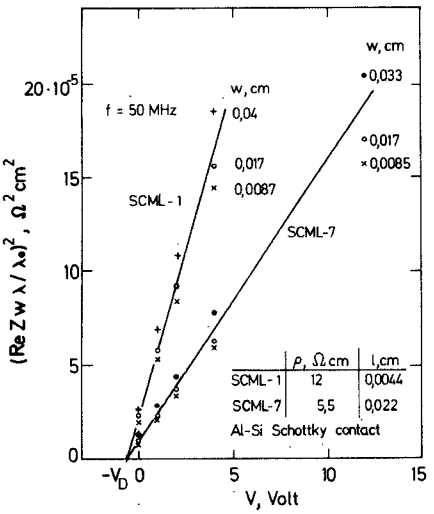

Fig. 6. Experimental determination of n_D and V_D.

number of approximations during analysis and the errors in measurement.

The transmission-line parameters are bias-dependent. Fig. 6 shows the measured reverse-voltage characteristics of six different SCML's within the slow-mode region. From (19) and (20) it is seen that the product

$$(\mathrm{Re}\ Zw\lambda/\lambda_0)^2 = \frac{2\varepsilon_0 Z_0^2}{en_D\varepsilon_r}(V + V_D)$$

is proportional to the sum of reverse bias V and barrier potential V_D of the Schottky barrier. Thus the intercept of the voltage axis yields $V_D = 0.6$ V and the slopes the doping concentrations n_D(SCML-1) $= 3.8 \cdot 10^{14}$ cm^{-3} and n_D(SCML-7) $= 8.9 \cdot 10^{14}$ cm^{-3}, in excellent agreement with the resistivities determined by the four-point probe measurements.

In Figs. 7 and 8 the admittance curves of series impedance $W' = \gamma Z$ per unit length and shunt admittance $Y' = \gamma/Z$ are given, respectively. In Fig. 7, W' consists of an inductance in series with a nearly frequency-independent resistance. No bias dependence is observed within experimental error. A quantitative agreement with the equivalent network of Fig. 3 is obtained when L' is calculated from the given parameters on the basis of real microstrip configuration. Re W_m' is then identified with the measured HF resistance of the conductors. It is evident that the internal inductance Im W_m' can be neglected in comparison with the external L' and that the longitudinal losses within the semiconductor may also be ignored: Re $W_m' \gg \omega^2 L'^2/R'$. The values of $-45°$ frequencies determine the lower limit f_{m2}, (23).

The measured shunt admittance Y' (Fig. 8) is that of the Schottky-barrier diode, the depletion-layer capacitance C_2' in series with the bulk conductance G_1'. The values of the 45° frequencies correspond with the upper limit f_c of the slow-mode region. Since l_2 of the SCML is bias-dependent, the frequency markers shift to the origin with increasing bias, resulting in larger values of f_c, (1), (14), and (15). Thus Figs. 7 and 8 show that TM slow-wave

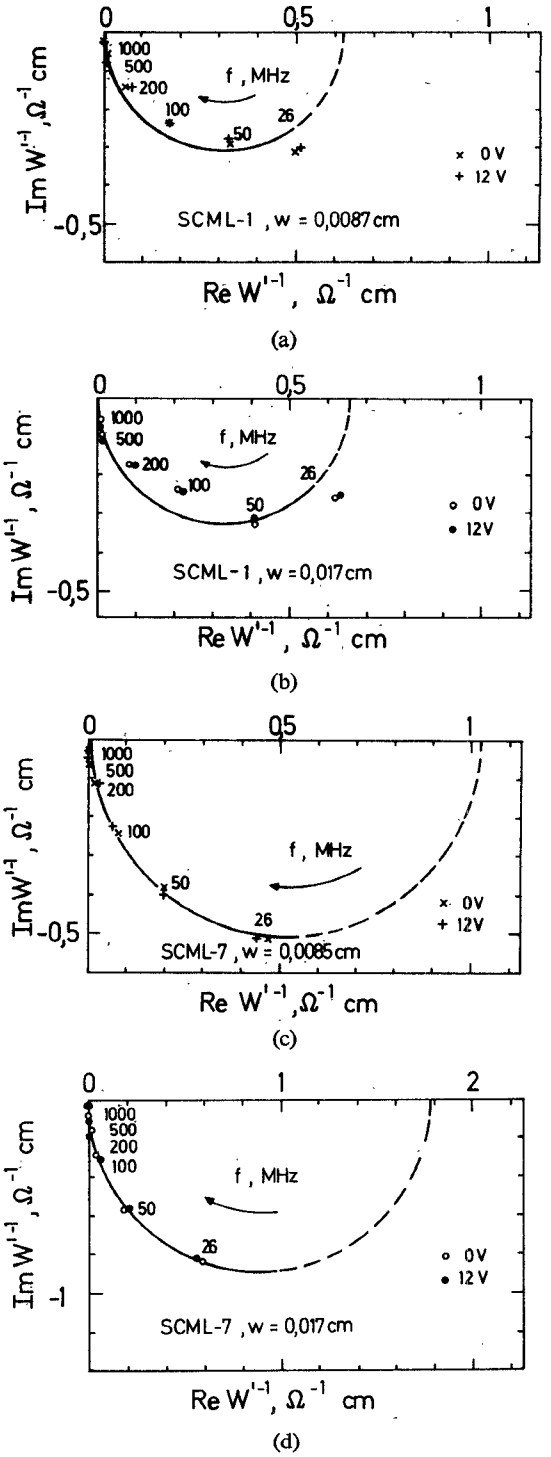

Fig. 7. (a)–(d) Measured admittance curves of series impedance $W' = \gamma Z$; parameter is the bias.

propagation along the SCML may be described by the equivalent circuit of Fig. 3 even in the microstrip case.

Slow-wave propagation on the Si–SCML's is shown in Fig. 9. Phase velocity and delay time T are calculated from (19). For example, a SCML on an n–Si substrate, of typical thickness 0.02 cm, exhibits phase velocities $v \lesssim 0.01c$ for resistivities $\rho \lesssim 0.1\ \Omega \cdot$ cm. Furthermore, a bias variation from 0 to 12 V changes v by more than a factor of 2. Experimental points are also plotted in Fig. 9.

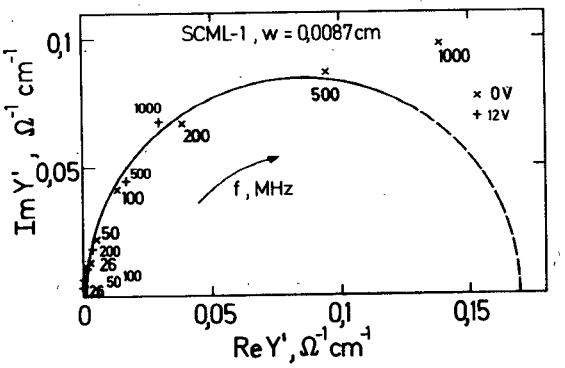

(a)

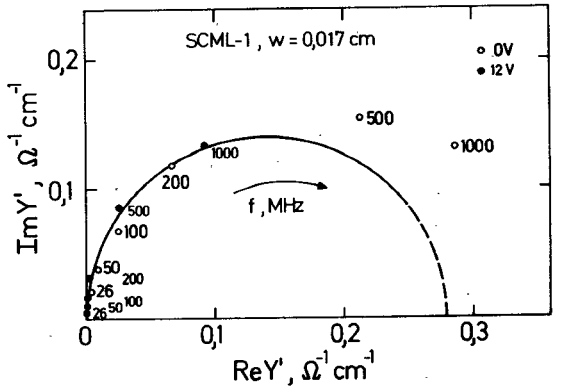

(b)

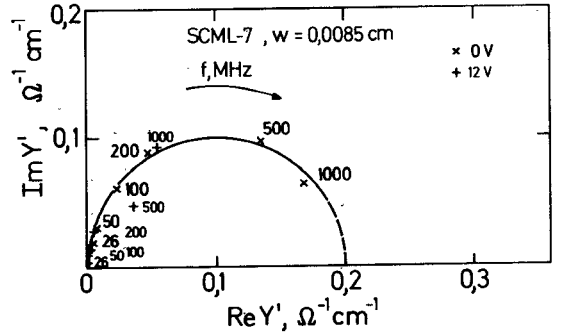

(c)

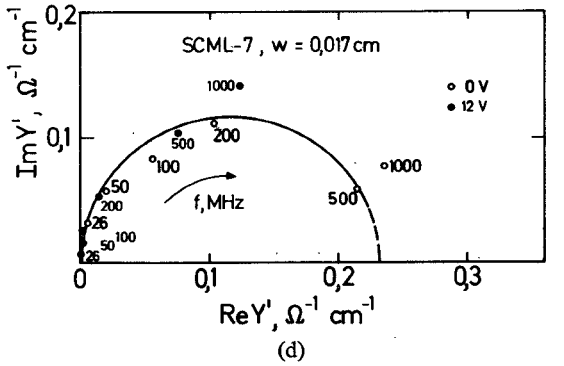

(d)

Fig. 8. (a)–(d) Measured admittance curves of shunt admittance $Y' = \gamma/Z$; parameter is the bias.

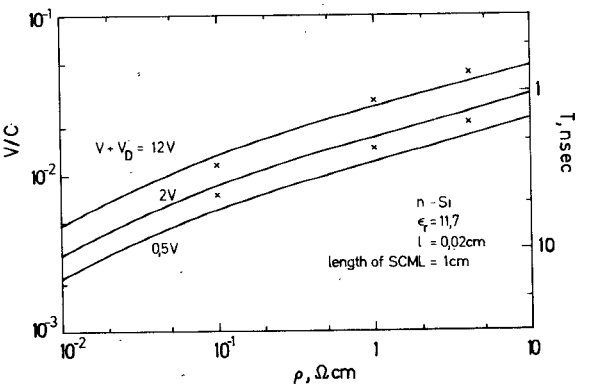

Fig. 9. Phase velocity and delay time of SCML as a function of semiconductor resistivity.

V. Summary and Conclusions

Slow-wave propagation on the SCML's is investigated both theoretically and experimentally, and the frequency limits are given. The upper one results from the frequency limit for interfacial polarization, while the lower one is determined by finite conductivity of the metallic conductors. Formulas for the characteristic impedance and propagation constant are derived together with an equivalent circuit. The analysis is confirmed by experiments performed on the SCML's on the n–Si substrate with Al–Si and Au–Si Schottky contacts.

The fundamental nonlinear properties of the SCML's, together with the very low phase velocity, are the most attractive features for possible applications in IC-microwave components with variable parameters. Such components would be of very small size due to highly reduced guide wavelength. The presented results, however, show clearly the dominating influence of imperfect conductors. This influence cannot be neglected when designing SCML's as well as microstrip lines on MOS systems with optimum performance. Therefore, practical applications are only feasible if optimum stripline parameters are given. These parameters, e.g., substrate thickness, mobility and doping concentration of a suitable semiconductor, Schottky-barrier potential, and strip width, may be calculated from the formulas of Section III. Beyond that, the presented equations and equivalent circuit are also valid if the depletion layer is realized by a p-n-junction, for example, and the theoretical treatment may be employed when similar microstrip lines are analyzed where the cross section equals any other semiconductor diode used in microwave techniques.

Acknowledgment

The author wishes to thank Prof. W. Hampe of the Institute for Applied Physics, University of Münster, for many helpful discussions and his assistance during the course of this work.

References

[1] W. Rabus, "Über die Frequenzvervielfachung längs Schottky-Kontakt-Leitungen," *AEÜ*, vol. 28, pp. 1–11, Jan 1974; also thesis, University of Erlangen-Nürnberg, Germany, 1973.

[2] K. Everszumrode, B. Brockmann, and D. Jäger, "Über den Wirkungsgrad der Frequenzvervielfachung längs Schottky-Kontakt-Leitungen," in preparation.
[3] D. Jäger and W. Rabus, "Bias-dependent phase delay of Schottky contact microstrip line," *Electron. Lett.*, vol. 9, pp. 201–202, May 1973.
[4] D. Jäger, W. Rabus, and W. Eickhoff, "Bias-dependent small-signal parameters of Schottky contact microstrip lines," *Solid-St. Electron.*, vol. 17, pp. 777–783, Aug. 1974.
[5] D. Jäger, "Wellenausbreitung auf Schottky-Kontakt-Leitungen im Kleinsignalbetrieb," thesis, University of Münster, Germany, 1974.
[6] W. Schäfer, J. P. Becker, and D. Jäger, "Variable Tiefpassfilter in Streifenleitungstechnik," in preparation.
[7] D. Jäger and W. Rabus, "Elektrische Leitung auf halbleitendem Substratmaterial," patent pending, 1973.
[8] H. Guckel, P. A. Brennan, and I. Palocz, "A parallel-plate waveguide approach to microminiaturized planar transmission lines for integrated circuits," *IEEE Trans. Microwave Theory Tech.*, vol. MTT-15, pp. 468–476, Aug. 1967.
[9] I. T. Ho and S. K. Mullick, "Analysis of transmission lines on integrated circuit chips," *IEEE J. Solid-St. Circuits*, vol. SC-2, pp. 201–208, Dec. 1967.
[10] H. Hasegawa and H. Yanai, "Characteristics of parallel-plate waveguide filled with a silicon-siliconoxide system," *Electron. and Commun. Jap.*, vol. 53-B, no. 10, pp. 63–73, 1970.
[11] H. Hasegawa, M. Furukawa, and H. Yanai, "Properties of microstrip line on Si–SiO_2 system," *IEEE Trans. Microwave Theory Tech.*, vol. MTT-19, pp. 869–881, Nov. 1971.
[12] J. M. Jaffe, "A high frequency variable delay line," *IEEE Trans. Electron Devices*, vol. ED-19, pp. 1292–1294, Dec. 1972.
[13] U. Günther and E. Voges, "Variable capacitance MIS microstrip lines," *AEÜ*, vol. 27, pp. 131–139, March 1973.
[14] S. M. Sze, *Physics of Semiconductor Devices*. New York: Wiley-Interscience, 1969.
[15] R. E. Collin, *Field Theory of Guided Waves*. New York: McGraw-Hill, 1960.
[16] a) R. A. Pucel, D. J. Masse, and C. P. Hartwig, "Losses in microstrip," *IEEE Trans. Microwave Theory Tech.*, vol. MTT-16, pp. 342–350, June 1968.
b) ——, "Correction to 'Losses in microstrip'," *ibid.* (Corresp.), vol. MTT-16, p. 1064, Dec. 1968.

Analysis of a Waveguide Mounting Configuration for Electronically Tuned Transferred-Electron-Device Oscillators and its Circuit Application

J. S. JOSHI AND J. A. F. CORNICK

Abstract—**Theoretical analysis of a waveguide-post mounting configuration employed for high electronic (varactor) tuning of a transferred-electron-device oscillator is presented. The resulting two-port-coupling network representation is also used to derive the impedance of the post structure as an obstacle to the dominant TE_{10} mode in the waveguide. Obstacle measurements conducted on the post structure for the incident TE_{10} mode are found to be in very good agreement with the theory.**

This network representation is then applied to a practical transferred-electron-device oscillator reported elsewhere. It has been able to successfully explain the characteristic features of the oscillator. It is observed that the main source of discrepancy between the theoretical and experimental characteristics could be attributed to a lack of knowledge of the precise values of the package parasitic elements. The nature of the theoretical varactor-tuning characteristic predicted by the model is discussed and indicated for a particular configuration.

Introduction

ELECTRONICALLY TUNED transferred-electron oscillators are finding increasing practical applications. There are mainly two elements which can be used for electronic tuning of transferred-electron-device oscillators, namely YIG elements and varactor diodes. Although YIG-tuned transferred-electron oscillators are capable of providing a large electronic tuning range [1] (of the order of an octave), they are not favored in most systems applications because of their sluggish dynamic response. Varactor diodes, on the other hand, have a very fast dynamic response and are therefore more frequently used in the systems demanding fast response rates.

However, for good noise performance, it is also desirable that such varactor-tuned transferred-electron-device oscillators be constructed in relatively high-Q configurations. Standard-height waveguide cavities provide such configurations. The first published results on a varactor-tuned transferred-electron oscillator in a full-height waveguide cavity [2] reported an electronic tuning range of over 1 GHz in X band. This configuration utilized post mounting arrangements in which the transferred-electron device and the varactor diode were mounted on separate posts at the opposite ends of the waveguide height. The posts were located as close as is mechanically possible to maximize the degree of coupling between the two devices. In the limiting case when the two posts merge, that is, when the devices are located at the opposite ends of the same post, one would expect an even greater electronic tuning range. Such a configuration [Fig. 1(a)] has been utilized to obtain large electronic tuning ranges [3], [4].

It is the aim of this paper to characterize such mounting configurations in the form of a multiport network. This network will be used to explain the experimentally observed results [4].

Manuscript received April 30, 1975; revised March 15, 1976.
The authors are with Mullard Hazel Grove Ltd., Bramhall Moor Lane, Hazel Grove, Cheshire SK7 5BJ, England.